Accepted Manuscript

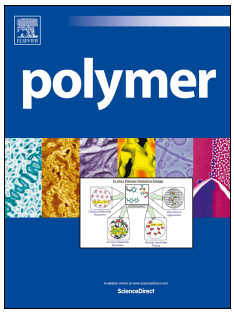

Influence of the cross-linker content on adsorbed functionalised microgel coatings

Tetyana Kyrey, Judith Witte, Vitaliy Pipich, Artem Feoktystov, Alexandros Koutsioubas, Egor Vezhlev, Henrich Frielinghaus, Regine von Klitzing, Stefan Wellert, Olaf Holderer

PII: S0032-3861(19)30168-5

DOI: https://doi.org/10.1016/j.polymer.2019.02.037

Reference: JPOL 21276

To appear in: *Polymer*

Received Date: 19 September 2018

Revised Date: 15 February 2019

Accepted Date: 18 February 2019

Please cite this article as: Kyrey T, Witte J, Pipich V, Feoktystov A, Koutsioubas A, Vezhlev E, Frielinghaus H, von Klitzing R, Wellert S, Holderer O, Influence of the cross-linker content on adsorbed functionalised microgel coatings, *Polymer* (2019), doi: https://doi.org/10.1016/j.polymer.2019.02.037.

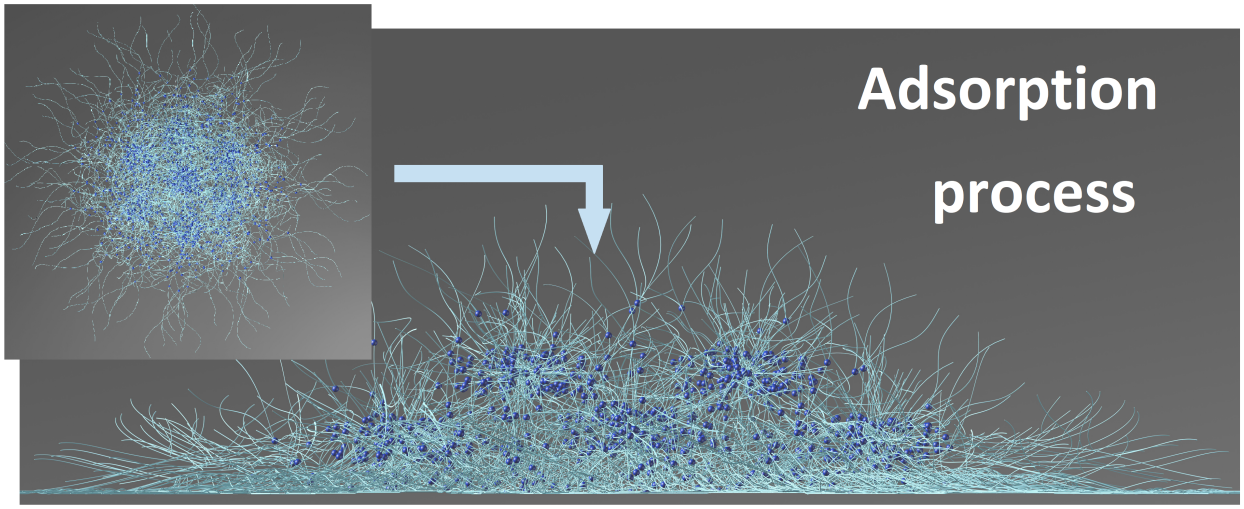

Influence of the cross-linker content on adsorbed functionalised microgel coatings

Tetyana Kyrey[1,2], Judith Witte[1], Vitaliy Pipich[2], Artem Feoktystov[2], Alexandros Koutsioubas[2], Egor Vezhlev[2], Henrich Frielinghaus[2], Regine von Klitzing[3], Stefan Wellert[1], Olaf Holderer[2]*

[1]Technical University Berlin,

Stranski-Laboratory for Physical and Theoretical Chemistry,

Str. des 17. Juni 124, 10623 Berlin, Germany

[2]Forschungszentrum Jülich GmbH,

Jülich Centre for Neutron Science at MLZ,

Lichtenbergstraße 1, 85748 Garching, Germany

[3]Technical University Darmstadt,

Department of Physics, Soft Matter at Interfaces,

Alarich-Weiss-Strasse 10, 64287 Darmstadt, Germany

Corresponding author: Tetyana Kyrey (t.kyrey@tu-berlin.de)

Stranski-Laboratory for Physical and Theoretical Chemistry, Institute of Chemistry,

Technical University Berlin, Sekr. TC 9, Str. des 17. Juni 124, 10623 Berlin, Germany

Present address:

Forschungszentrum Jülich GmbH, Jülich Centre for Neutron Science at MLZ,

Lichtenbergstr. 1, 85748 Garching, Germany

Tel.: +49-89-289-10778

Fax: +49-89-289-10799

ABSTRACT

The tunable properties of stimuli-responsive polymer coatings at solid surfaces inspire their application in different electronic devices, as functional tissue in regenerative medicine or even for drug release. Especially promising is the exploitation of thermo-responsive poly-*N*-isopropylacrylamide (PNIPAM) microgels as cell-surface adhesion control systems. In this context we present a morphological and internal structure investigation of thermo-responsive PNIPAM microgels adsorbed on a silicon-surface. By means of Grazing Incidence Small-Angle Neutron Scattering and Atomic Force Microscopy the swelling behaviour of adsorbed PNIPAM microgel particles and the influence of the *N,N'*-methylenebisacrylamide (cross-linker) content in the microgel network on the layer formation were investigated. The influence of the surface confinement on the responsivity of the polymer system is discussed.

Keywords: GISANS, PNIPAM, Surface confinement, internal inhomogeneities

1. INTRODUCTION

In the last few decades numerous works were dedicated to the investigation of stimuli-responsive or so called 'smart' polymer systems [1,2]. Currently, stimuli responsive surface structures attract much scientific interest due to their unique physical properties and the resulting large variety of envisioned applications. The possibility to arrange microgel particles of various compositions into one- and two-dimensional arrays inspires a series of technological applications in the field of soft nanotechnology utilizing their stimuli-responsive behaviour. For example, some research aims at the use of microgels in biotechnical and medical applications [3–5]. Here, the search for stimuli-responsive and biocompatible host and carrier media for a dedicated and controlled drug release on demand is underway. Such coatings could also improve the performance of implants such as neural electrodes [6]. Surfaces coated with PNIPAM are

promising for the construction of tissue for the control and adjustment of cell adhesion. It allows cell growth with high cell densities and the prevention of post-transplantation inflammation [7]. Such tissues permit the adhesion/detachment of the cell culture by a simple temperature switch. In this respect, cell adhesion and detachment were studied using coatings made from PNIPAM microgels [8–10]. Microgels in combination with metal nanoparticles are explored as building blocks for optical devices in nanooptics [1,11–14].

One pathway of preparing such surface structures is the controlled lateral arrangement of microgel particles, e.g. made of PNIPAM, at solid surfaces. The main feature of the PNIPAM microgels is the ability to change their degree of swelling due to change of external variables such as temperature, pH, light or solvent quality [4,15–21]. PNIPAM has a lower critical solution temperature (LCST) at 32 °C in water [22], i.e. the change of temperature allows to tune polymer properties (conformational from coil-to-globule transition). In general, microgels are colloidal particles consisting of a chemically cross-linked network structure. When dispersed in a good solvent, these particles are highly swollen with sizes ranging from 100 to 1000 nm. The synthesis by precipitation polymerization yields colloidal particles with a low polydispersity and allows the control of size, composition and functionalisation. Often, the chemical cross-linking in PNIPAM microgels is achieved by using *N,N'*-methylenebisacrylamide (BIS). Changing the cross-linker content tunes mean mesh size of the network and hence influences the swelling behaviour and the mechanical properties [23–26].

The lateral arrangement of microgel particles in a surface layer depends on substrate properties, particle deposition technique, solvent quality and microgel properties [25,27]. For example, the presence of the confining surface influences also the structure of the adsorbed poly(NIPAM-*co*-AAc) microgel particles. The microgel volume decreases by about one order of

magnitude during adsorption, which indicates a compression and densification of the microgels [28,29]. The attractive interactions between network and surface leading to deformation and compression of the polymer network inside the adsorbed microgel particles were discussed as possible reasons for the stiffening in the adsorbed state [30]. Recently, internal inhomogeneity inside adsorbed PNIPAM microgels by comparing core-shell and hollow microgels have been measured by AFM [31].

While the bulk properties of the PNIPAM microgels was thoroughly investigated by means of small-angle neutron or X-ray scattering (SANS/SAXS) and dynamic light scattering (DLS) [23,32–36], the understanding of the influence of the surface confinement on the internal structure of the adsorbed microgels is limited. An additional challenge in the study of such systems arises due to the small sample volume at the surface. Scattering experiments compliment imaging techniques and therefore, application of surface sensitive techniques like grazing incidence small-angle neutron scattering (GISANS) is of great interest.

The current work presents morphological and structural studies of the PNIPAM microgel adsorbed on a Si-block by means of AFM and surface sensitive GISANS. We have focused on the investigation of the PNIPAM microgel particles with low and medium cross-linker content (BIS – 0.5 and 5 mol %) at temperatures below and above the volume phase transition temperature (VPTT). The influence of the surface confinement and the cross-linker content on the swelling behaviour and the morphology and the structure of the polymer layer at silicon surface are presented.

2. MATERIALS AND METHODS

N-isopropylacrylamide (≥99%) (NIPAM), *N*,*N*'-methylenebisacrylamide (≥99.5%) (BIS) 2,2'-azobis(2-methylpropionamidine) dihydrochloride (97%) (AAPH) and poly(ethyleneimine)

(~50% in H_2O) (PEI) were purchased from Sigma-Aldrich (Munich, Germany). All chemicals were used as received. A Millipore Milli-Q Plus 185 purification system was used for water purification.

2.1. Microgel synthesis

Microgel particles based on the monomer *N*-isopropylacrylamide (NIPAM) and the cross-linker *N*,*N*'-methylenebisacrylamide (BIS) were synthesised via surfactant-free precipitation polymerisation. The amount of the cross-linker varied between 0.5mol% and 5 mol%. For simplification, we introduce the abbreviation PB_x, where P is PNIPAM, B is BIS and x the amount of the cross-linker in the system (0.5 or 5 mol %).

NIPAM (1.688 g, 14.9 mmol ($PB_{0.5}$); 1.613 g, 14.3 mmol (PB_5)) and BIS (0.012 g, 0.075 mmol ($PB_{0.5}$); 0.115 g, 0.75 mmol (PB_5)) were dissolved in 120 ml of water in a batch reactor. The solution was heated to 80° C and degassed with nitrogen for 60 min. Afterwards 1 ml of an aqueous solution of AAPH (0.25 mM) was added to the mixture while stirring continuously at 1000 rpm. After 10 min the reaction was quenched with an ice bath. For purification, the microgel particles were dialysed for 2 weeks with two water exchanges per day and freeze-dried at -85°C and 1 x 10^{-3} bar for 7 days.

2.2. Microgel deposition

Single crystal silicon blocks (50 x 80 x 15) mm with a surface roughness <1% at the (111) surface (Holm Siliciubearbeitung, Germany) were successively cleaned with acetone, ethanol and water and were dried under nitrogen flow. Afterwards, they were stored in an aqueous poly(ethyleneimine) (PEI) solution (0.01 g/mL) for 60 min and subsequently rinsed with water and dried under nitrogen flow. Microgels were deposited onto the PEI-coated silicon blocks via spin coating for 150 s with 500 rpm from aqueous microgel dispersion (0.01 g/mL). For AFM

imaging the microgel dispersion was spin coated with identical parameters onto silicon wafers of (20 x 20) mm.

2.3. Experimental techniques

2.3.1. Sample environment

All samples were mounted in an in-house produced thermostated cell [37]. With a Teflon trough inside aluminium housing the sample was sealed against air. To achieve the largest scattering contrast with the protonated microgels, the cell was filled with deuterated water (D_2O). Temperature control of ± 0.1°C inside the cell was achieved by water circulation through the aluminium housing. All samples were measured at 20°C and 50°C. These temperatures were chosen to observe the behaviour of the microgel particles below and above the VPTT.

The cell was mounted on a goniometer stage to achieve the necessary angle of incidence. The neutron beam entered the sample through the silicon block. To reduce the background and block the direct neutron beam Cd shieldings at the entrance and exit sides were used.

2.3.2. AFM

Atomic force microscopy (AFM) imaging was performed under ambient conditions with an Asylum Cypher at room temperature. The samples were scanned in the intermittent contact mode with a silicon cantilever (OMCL-AC160TS) with a spring constant of 26 N/m and a resonance frequency of 300 kHz. The chosen scan size was 20 x 20 µm. For image analysis the MFP3D software was used.

2.3.3. Grazing incidence small-angle neutron scattering

GISANS experiments were carried out at the KWS-1 [38,39] and the KWS-3 [40] instruments operated by the JCNS at the MLZ (Garching, Germany). The measurements were performed at a

sample-to-detector distance of 20 m using an unpolarised, monochromatic incident beam with a neutron wavelength of λ = 5Å ($\Delta\lambda/\lambda$ = 10%) at KWS-1 and 10 m and 12.8 Å at KWS-3 ($\Delta\lambda/\lambda$ = 20%). KWS-1 is a classical small-angle instrument, while KWS-3 is a very small-angle diffractometer and is optimised for measurements in the low Q-range. Using both instruments allows covering a wide Q-range of $3x10^{-5}$ – $2x10^{-2}$ $Å^{-1}$ and probing features from a few nano- to micrometres, i.e. from the internal structure of microgels to the external size and order parameter. To obtain the internal structure of the microgel particles all GISANS measurements were performed below the critical angle of total reflection of the microgel layer. Since the critical angle of total reflection α_c depends on neutron wavelength λ and scattering length density ρ as $\alpha_c(\lambda) = \lambda\sqrt{\rho/\pi}$, incident angles of 0.2° at λ = 5Å and 0.51° at λ = 12.8 Å were chosen at KWS-1 and KWS-3 respectively.

Fig. 1 represents the geometry of GISANS experiments and schematically depicts a model of the studied systems. The technique probes the structure at the solid-liquid interface. The neutron beam with wave vector $\boldsymbol{k_i}$ enters through the silicon block the surface layer at the silicon-water interface under a shallow incident angle α_i. The scattered intensity with wave vector $\boldsymbol{k_f}$ is than collected by a 2D detector as a function of the exit (α_f) and out-of-plane (ψ) angles [41,42]. For the characterisation of the microgel systems in the lateral direction horizontal line cuts were performed at the position of Yoneda peak (Y). A detailed description of the principles of the GISANS experiment can be found elsewhere [41–45]. GISANS data treatment was performed with the QtiKWS10 software package.

Due to the small sample volume and the strongly collimated neutron beam, the scattering signal in grazing incidence geometry has low intensity compared to the SANS measurements on bulk samples. Two experimental conditions were probed to find an optimal combination of

resolution and intensity: (i) higher angular resolution in lateral direction at lower beam intensity (the neutron beam was strongly collimated to the beam width of 15 mm; (ii) slits were opened to 48 mm in order to get more scattering intensity. Independent of the experimental set up, the same values for the lateral inhomogeneities were obtained, i.e. the results are not limited by the resolution (see Discussions). Each measurement was performed during 8 hours.

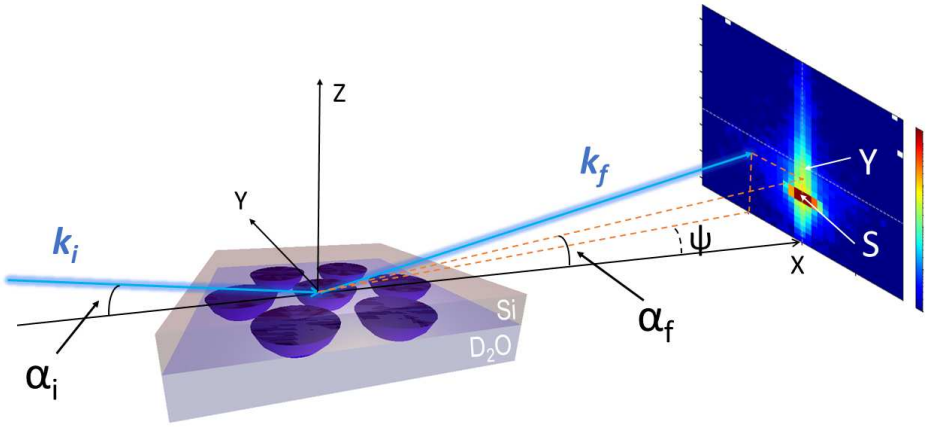

Figure 1. Schematic illustration of the scattering geometry under grazing incidence conditions. α_i – incident angle of the neutron beam with incident wave vector $\boldsymbol{k_i}$. A two-dimensional detector is used to measure the specular (S) and diffuse scattering (with wave vector $\boldsymbol{k_f}$) intensity as a function of exit angle α_f and the out-of-plane angle ψ. The horizontal line cut performed at the position of the Yoneda peak (Y) was used for data analysis.

2.4. Theoretical model

Due to the distribution and incorporation of the cross-linker molecules during the preparation process, different types of polymer inhomogeneities in the microgel are formed [46]. According to Bastide and co-workers [47], the microgel network could be described in the framework of the mesh model. In this model, the combination of blobs and their connection with each other corresponds to the cross-linkers and PNIPAM chains respectively. Above the VPTT, the

PNIPAM chains are collapsed and the cross-linker distribution is not detectable. The decrease of the temperature and the swelling process lead to the formation of domains with frozen neighbour-junctions which do not swell homogeneously (Fig. 2). These domains become visible and detectable in neutron scattering below the VPTT, where swelling with the constraints of the cross-links leads to the inhomogeneous polymer chain conformations in the microgel particles. The precipitation polymerisation used for sample produce leads to an inhomogeneous distribution of the cross-links due to the polymerisation kinetics (different VPTT for PNIPAM and BIS). In the frame of the mesh model, all internal concentration fluctuations can be described in terms of thermal fluctuations and static inhomogeneities.

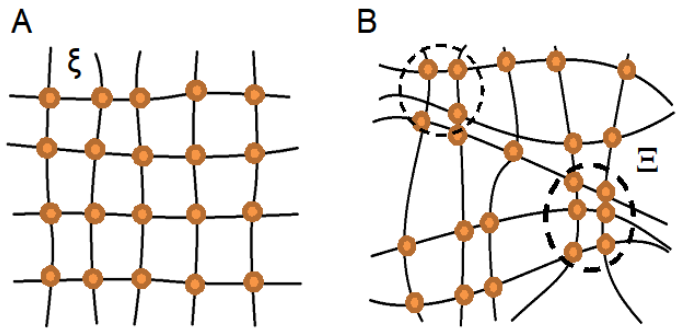

Figure 2. Illustration of the mesh model according to Ref. [46,47]: A) a two-dimensional reaction bath well above the chain gelation threshold, B) an swollen gel by the addition of solvent. The orange dots represent interchain cross-links. Dashed-circles depict domains with frozen neighbour-junctions which do not swell.

The simplest description of each component is a sum of Ornstein-Zernike (1) and Debye-Bueche (2) functions. The first one represents thermal fluctuations on a very local scale inside the microgel particles and corresponds to the higher Q-range, while the second one describes the frozen inhomogeneities, which are detectable at smaller Q:

$$F_{therm}(Q) = \frac{I_{oz}}{1+\xi^2 Q^2} \quad (1)$$

$$F_{froz}(Q) = \frac{I_{inh}}{(1+\Xi^2 Q^2)^2} \quad (2)$$

where ξ is the correlation length, Ξ – the characteristics size of the inhomogeneities, I_{oz} and I_{inh} – the scattering signal from the thermal fluctuations and frozen inhomogeneities at Q_0.

Assuming Gaussian to describe the experimental resolution function, the model for quantitative description is given by

$$F(Q) = Aexp\left(-\frac{(Q-Q_{max})^2}{2\sigma^2}\right) + \frac{I_{inh}}{(1+\Xi^2 Q^2)^2} + \frac{I_{oz}}{1+\xi^2 Q^2} + I_{Bgd} \quad (3)$$

where A is an amplitude, Q_{max} = 0 – the position of the peak maximum, σ – FWHM represents the instrumental resolution, I_{Bgd} represents the incoherent scattering background. Figure 3 depicts the contribution of each fitting component.

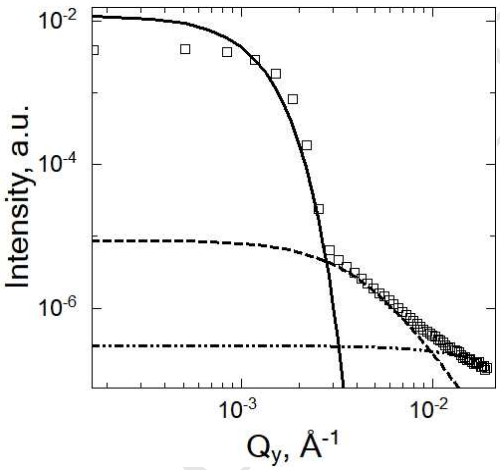

Figure 3. Contribution of the different terms in Eq.3: the solid line corresponds to the Gaussian resolution part, dashed line to the Debye-Bueche function with $\Xi \sim 230$ Å and the dash-dotted line to the Ornstein-Zernike function ($\xi \sim 50$ Å).

3. RESULTS

3.1. Morphological characterisation of the adsorbed microgel particles

Initial characterisation of the microgel particles after adsorption was done by AFM measurements. The AFM images of PB_5 and $PB_{0.5}$ as well as the cross section of one individual particle in dry state are presented in Fig. 4 (liquid AFM images show the same particle distribution on local scales for PB_5, while for $PB_{0.5}$ an experiment is not feasible)).

In case of PB_5 the individual particles are clearly visible on the Si-surface. Figure 4A displays a AFM image with a scan size of 20 x 20 µm overview of PB_5. Here areas with different particle-particle distances was observed. In case of PB_5 a total number of 459 individual particles was analysed (edge particles were ignored) and the geometrical parameters can be found in Table 1.

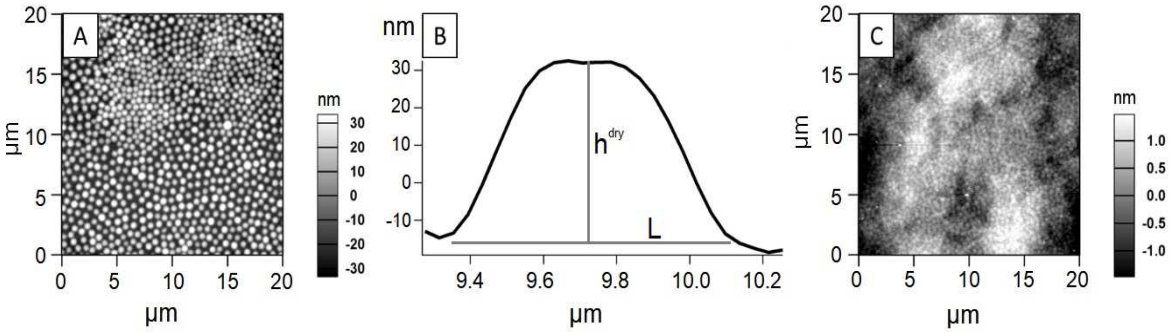

Figure 4. A) AFM image of adsorbed PB_5, B) profile of one of the microgel particle from AFM image A, C) AFM image of adsorbed $PB_{0.5}$. The samples were scanned at room temperature in the collapsed state under dry conditions.

From the AFM image analysis the geometrical parameters of PB_5 were determined: the height of the particle in the dry and wet state are h^{dry} = (39.1 ± 7.5) nm and h^{wet} = (120 ± 57) nm, respectively, the averaged width is L = (507 ± 102) nm. In contrast to PB_5 due to the small height of the $PB_{0.5}$ the individual microgel particles are not detectable, and the AFM image

analysis for $PB_{0.5}$ was not feasible (Fig. 4C). The comparison of the particle parameters in bulk and in adsorbed state as well as hydrodynamic radii and internal microgel parameters are presented in Table 1 (for details of DLS and SANS measurements see in ESI).

Table 1. Radius of the microgel particles and mesh size of polymer network ξ_{bulk} in bulk (DLS, SANS) and the parameters of individual particle, namely width of adsorbed microgel particle (AFM), mesh size of polymer network ξ_{surf} and characteristic size of inhomogeneities Ξ_{surf} in the adsorbed state (GISANS, see section 3.3.1). In parentheses standard deviation is indicated.

System	$R_{DLS}^{T=20°C}$, nm	$R_{SANS}^{T=20°C}$, nm	L_{AFM}, nm	Ξ_{surf}, nm	ξ_{surf}, nm	ξ_{bulk}, nm
$PB_{0.5}$	265 (1.9)	-	-	22.7 (1.4)	5.7 (0.07)	3.5 (0.04)
PB_5	350 (1.5)	136.6 (1.6)	507.1 (102.5)	23.9 (2.2)	4.7 (0.07)	3.6 (0.02)

3.3. Structure of the adsorbed microgels: GISANS

3.3.1. Internal structure ($Q = 10^{-3} – 2x10^{-2}$ Å^{-1})

Lateral behaviour and internal structure of the adsorbed microgel systems $PB_{0.5}$ and PB_5 were studied below and above the VPTT by means of the GISANS technique. While the maximal scattering information about the studied system's structure is at the position of the Yoneda peak [42], which corresponds to the critical angle of total reflection, horizontal line cuts of the 2D detector images at Q_z corresponding to α_c (Fig.5 inset) were performed to characterise the internal structure of the microgel particles.

In Fig.5 the 2D-detector image of the $PB_{0.5}$ as well as the horizontal line cuts of the 2D GISANS data of $PB_{0.5}$ and PB_5 in the swollen and collapsed state are presented. For better visualisation data at 50°C were multiplied by a factor 10. Here, dashed lines represent plots according to equation (3). By means of the mesh model the characteristic correlation length ξ and the size of the inhomogeneities Ξ for both systems were determined (Table 1).

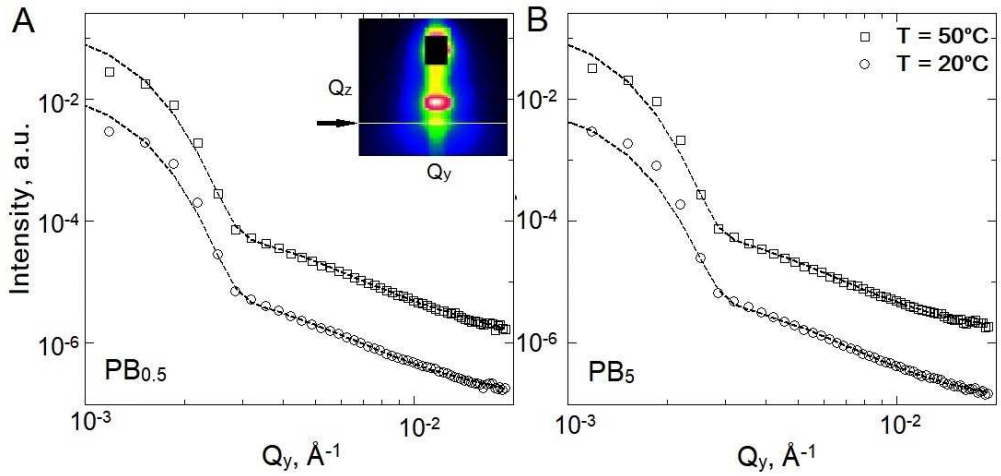

Figure 5. Horizontal line cuts of the 2D GISANS data of the PNIPAM microgel particles cross-linked with 0.5 mol% BIS (A) and 5 mol% BIS (B). The dashed lines represent fits according to Eq. 3. The curves were shifted along the Y-axis for the sake of clarity. In the inset the 2D detector image with the cut at the position of the Yoneda peak is indicated.

Increase of the temperature does not alter of the shape of the line cuts and therefore changes of the correlation lengths were not detectable. The correlation length ξ for $PB_{0.5}$ and PB_5 yields 5.7 nm and 4.7 nm respectively. The characteristic size of the frozen inhomogeneities Ξ is 23-24 nm for both systems according to the fit to the cut lines.

3.3.2. Lateral ordering of microgel particles on a Si-surface (Q = 3 x 10^{-5} – 2 x 10^{-3} Å^{-1})

To characterise larger structures, a GISANS measurement with higher resolution in the low Q-range was performed. In Fig. 6 the horizontal line cuts of 2D-detector images of $PB_{0.5}$ and PB_5 at 20°C and 50°C are presented. While for the system with 0.5 mol % BIS only the increase of intensity with the temperature is observed, in case of PB_5 an additional peak appears above the VPTT at Q_y = 7.8 x 10^{-4} Å^{-1}. The low intensity and smearing of the appearing peak is attributed to the position distribution of the particles on the solid surface, i.e. the inter-particle distances are

shorter in the centre region of the block (as in Fig. 4C), while the inter-particle distances in the outer part are larger.

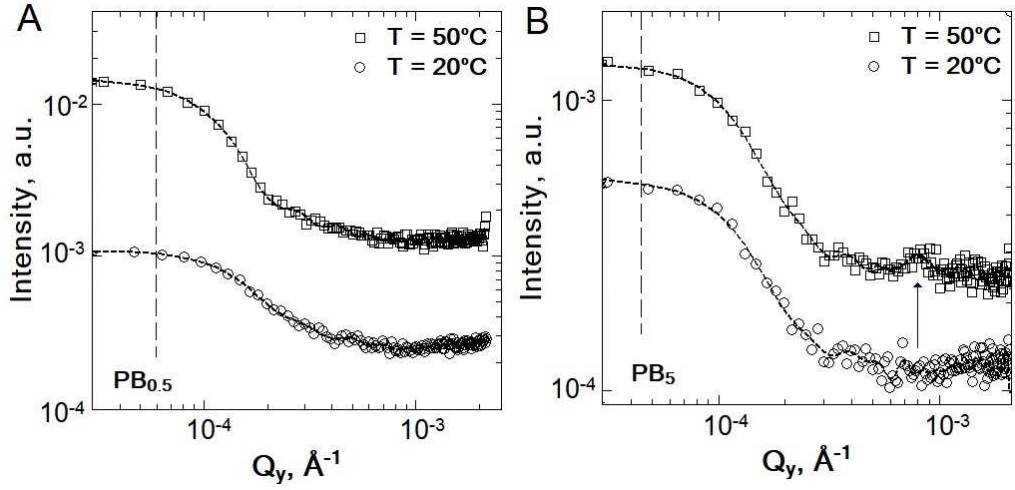

Figure 6. Horizontal line cuts of the 2D intensity distribution of the system $PB_{0.5}$ (A) and PB_5 (B) at temperatures above and below VPTT. The curves were shifted for the sake of clarity. Lines are the guides for the eye. The vertical dashed line indicates the resolution limit. Errors are <15% in the whole q-range.

In real space, the position of the peak maximum corresponds to a characteristic length $d \approx 805$ nm. Taking into account the particle parameters from the AFM measurements, we attribute the parameter d to a averaged distance between individual microgel particles. Two possible explanations of the second peak, appearing above the VPTT, can be considered. The first one takes into account the possibility of free PNIPAM dangling ends of the neighbouring particles to intersect with each other in the swollen state. It smears out the outer contour of the individual particles on the surface at 20°C and only the temperature increase and the related chain collapse lead to the additional peak in the GISANS scaling curve at 50°C. In case of layers with mean interparticle distances much larger than the mean particle lateral distance (non-dense

packing) such chain intersection is negligible. The second explanation is based on the PNIPAM transition from hydrophilic to less hydrophilic across its LCST. Below the VPTT the PNIPAM particles are in the swollen state, thus a high amount of water inside the particles decreases the scattering contrast between particles and bulk water and only after the temperature increase and water expulsion the collapsed particles become detectable in GISANS experiments. The first explanation is unlikely due to the strong lateral confinement of the free segments of the dangling ends.

In case of the system $PB_{0.5}$, the microgels present a layer-like structure on the Si-surface and even an increase of the temperature does not lead to the particle separation.

4. DISCUSSION

The investigation of the adsorbed PNIPAM microgel particles with AFM and GISANS provided structural information at different length scales.

It was found, that the main difference in film quality consists in an ability to arrange separated particles on the solid surface. The crosslinker concentration influences the stiffness and deformability of the microgel particles [48]. Initially, in bulk the PNIPAM particles possess a core-shell-like structure with a cross-link gradient from the core with a high polymer density to a loosely cross-linked outer shell [4,33]. At low crosslinker concentration (0.5 mol%) fluffy microgel particles are formed and the adsorption process leads to strong deformations of the particles in vertical direction perpendicular to the substrate and the formation of the layer-like shape is observed. At 5 mol% crosslinker concentration the particles have a distinct heterogeneous structure and in the adsorbed state at a Si-surface individual and clearly separated particles are observed (Figure 4). The core region is slightly deformed, while the shell of the particles undergoes stronger deformation.

In the adsorption process, microgels are immobilised at the surface due to the attractive particle-surface interaction. The polymers are compressed normal to the surface ($h_{AFM}/R_{DLS} \approx 0.3$) and stretched in the lateral direction ($L_{AFM}/R_{DLS} \approx 1.45$), which results in the increase of ξ compared to the bulk (see Table 1). Due to the compression, the volume of the adsorbed PB_5 particles decreases by one order of magnitude as compared to the particles' volume obtained from DLS (see ESI). It is comparable to the volume from the SANS experiment (see ESI): $V_{AFM}/V_{DLS} \approx 1{:}10$, $V_{AFM}/V_{SANS} \approx 1{:}1$.

Thus, in case of PB_5 the denser core (according to R_{SANS}) of the particle constitutes the main part in the adsorbed state, whereas the shell of PB_5 as well as the much fluffier particles of $PB_{0.5}$ undergo strong adhesion toward the surface and acquire a plat layer-like structure with partially overlapping of polymer chain segments.

Such differences in layer formation are also in good agreement with theoretical predictions. According to Vilgis and co-workers [49] the adsorption behaviour of the gels is determined by the gain of energy under surface contact that leads to a gel spreading and deformation to some extent with a typical displacement and forms a footprint of extension *L*. This extension strongly depends on the molecular weight of the chains and becomes large for weakly cross-linked gels. If *L* is small, van der Waals forces may become important and thicken the footprint. In the context of solvent swollen gels at an initially dry interface, an additional interplay between the solvent molecules and the surface occurs. In this situation solvent can leak out from the gels and spread onto the surface, forming a thin film around the gel. Therefore, $PB_{0.5}$ with a lower cross-linker content and a more fluffy structure undergoes larger deformation. It leads to the overlapping of the PNIPAM chains from neighbouring particles and the formation of the layer-like structure. The higher cross-link concentration of PB_5 leads to the shorter lateral extension, i.e. mostly the

shell region of the particles undergoes significant deformation, and the well-defined individual particles are observable. The absence of the individual particles at the surface in case of 0.5 mol% BIS is confirmed by AFM (as shown in Figure 2C). It seems that due to the low amount of cross-linker in the system, free dangling PNIPAM chains bind physically to the surface of the Si-block during the preparation process. That might lead to the formation of a fluffy microgel layer instead of the layer of the individual particles as for PB_5.

The different type of the adsorbed polymer particles in the swollen state (individual particles at 5mol% BIS and smoothed layer at 0.5 mol% BIS) is also in agreement with the our neutron reflectometry measurements (see ESI). We showed that a scattering length density (SLD) profile in case of $PB_{0.5}$ has a step-like form, that corresponds to the layer-like structure with sharp transition to the water interface, whereas the SLD profile of PB_5 indicates a gradually increase of the water amount in the polymer layer perpendicular to the surface.

Although the AFM images of $PB_{0.5}$ are very smooth and an identification of individual particles is not possible, the internal structure and characteristic correlation length in case of 0.5 mol% BIS are detectable using GISANS. The correlation length of the polymer network in the adsorbed state is slightly larger compared to the bulk. The sections through the 2D intensity pattern provide the component ξ_{surf} parallel to the interface. The GISANS experiments further revealed the existence of frozen inhomogeneities with a length scale Ξ = 22.7 (23.9) nm for 0.5 (5) mol% BIS. The presence of characteristic domains inside the microgel particles was also recently confirmed by S. Matsui and co-authors [50]. They showed that a during temperature increase the microgels gradually contract, whereas domains of several tens of nanometer in size are present inside. The finding is in agreement with the values of Ξ obtained in our experiment. These domains persisted near the VPTT and did not disappear above VPTT.

Figure 7 sketches the adsorbed microgel particle with the characteristic internal density fluctuations and the waterless microgel layer in the vicinity to the Si-surface in case of 5 mol % cross-linker.

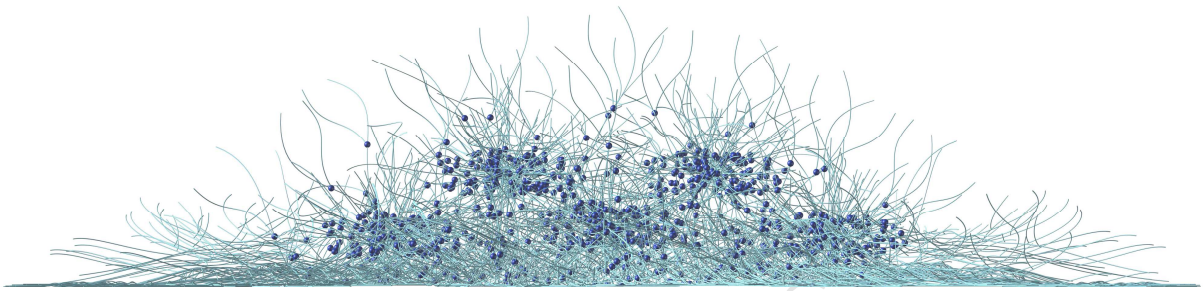

Figure 7. Model of the adsorbed microgel particle. The solid lines represent linear polymer chains, the cross-links are represented by the blue spheres.

A further point of interest is that the correlation length ξ as well as the characteristic size of the inhomogeneities Ξ are independent of the temperature in the adsorbed state, i.e. they remain constant above and below the VPTT for both systems. Consequently, the strong particle-surface interaction makes it hard to change the correlation lengths and so the internal structure of the adsorbed particles in the vicinity to the surface. Similar behaviour was recently reported for PNIPAM-co-AAc and PEG based microgel particles [29,30,51].

5. CONCLUSIONS

Using the combination of atomic force microscopy and grazing incidence small-angle neutron scattering over a broad Q-range allows a detailed characterisation of the lateral arrangements of adsorbed microgels in dependence on the temperature and cross-linker content in the adsorbed state.

In terms of the thermal fluctuations and static density or frozen inhomogeneities the characteristic correlation lengths ξ and Ξ were determined. We showed that the presence of the

surface strongly influences the properties of the adsorbed microgel particles and leads to an increase of the mesh parameter ξ by ~23% and ~40% in case of PB_5 and $PB_{0.5}$ respectively. The much flatter conformation of the microgels with low cross-linker content leads to a larger correlation length.

Moreover, the surface confinement strongly affects the temperature behaviour of the adsorbed microgels, i.e. the temperature increase does not lead to any significant structural changes of the microgel particles in lateral direction independent of the cross-linker amount.

While particle-surface interaction and particle-particle interaction determine the layer formation, the strong influence of the cross-linker content on the surface structure of the microgel layer was obtained. Due to the changed deformability of the microgels particles the formation of the well-defined individual particles could be detected for 5 mol % cross-linker, while at 0.5 mol % crosslinker the fuzzy gel layer was formed.

In the future, also the polymer chain dynamics of adsorbed microgel particles will be studied. Together with the structural investigations on length scales of the polymer chains up to length scales of whole particles a thorough understanding of all aspects of interface effects might pave the way for the design of new functionalized surface coatings.

ACKNOWLEDGEMENTS

We gratefully acknowledge funding by the Deutsche Forschungsgemeinschaft (DFG) [Grants HO 5488/2-1 and WE 5066/3-1]. T.K., J.W. and S.W thank JCNS and MLZ for the beam time and support to perform the neutron scattering measurements and P. Schöffman for support in AFM measurements.

Supplementary Information. The Electronic Supplementary Materia is available free of charge.

REFERENCES

[1] M. Karg, T. Hellweg, New "smart" poly(NIPAM) microgels and nanoparticle microgel hybrids: Properties and advances in characterisation, Current Opinion in Colloid & Interface Science. 14 (2009) 438–450. doi:10.1016/j.cocis.2009.08.002.

[2] W. Richtering, B.R. Saunders, Gel architectures and their complexity, Soft Matter. 10 (2014) 3695–3702. doi:10.1039/c4sm00208c.

[3] A.S. Hoffman, Hydrogels for biomedical applications, Advanced Drug Delivery Reviews. 64 (2012) 18–23. doi:10.1016/j.addr.2012.09.010.

[4] R. Pelton, Temperature-sensitive aqueous microgels, Advances in Colloid and Interface Science. 85 (2000) 1–33.

[5] E.S. Gil, S.M. Hudson, Stimuli-reponsive polymers and their bioconjugates, Prog. Polym. Sci. 29 (2004) 1173–1222. doi:10.1016/j.progpolymsci.2004.08.003.

[6] S.M. Gutowski, K.L. Templeman, A.B. South, J.C. Gaulding, J.T. Shoemaker, M.C. LaPlaca, R. V. Bellamkonda, L.A. Lyon, A.J. Garcia, Host response to microgel coatings on neural electrodes implanted in the brain, J. Biomed. Mater. Res., Part A. 102A (2014) 1486–1499. doi:10.1002/jbm.a.34799.

[7] M.A. Cooperstein, P.A.H. Nguyen, H.E. Canavan, Poly (N-isopropyl acrylamide) -coated surfaces: Investigation of the mechanism of cell detachment, Biointerphases. 12 (2017) 02C401.

[8] I. Lynch, I. Miller, W.M. Gallagher, K.A. Dawson, Novel Method to Prepare Morphologically Rich Polymeric Surfaces for Biomedical Applications via Phase Separation and Arrest of Microgel Particles, Journal of Physical Chemistry. 110 (2006) 14581–14589. doi:10.1021/jp061166a.

[9] S. Schmidt, M. Zeiser, T. Hellweg, C. Duschl, A. Fery, H. Möhwald, Adhesion and Mechanical Properties of PNIPAM Microgel Films and Their Potential Use as Switchable Cell Culture Substrates, Adv. Funct. Mater. 20 (2010) 3235–3243. doi:10.1002/adfm.201000730.

[10] H.-Y. Tsai, K. Vats, M.Z. Yates, D.S.W. Benoit, Two-Dimensional Patterns of Poly(N□isopropylacrylamide) Microgels to Spatially Control Fibroblast Adhesion and Temperature-Responsive Detachment, Langmuir. 29 (2013) 12183–12193. doi:10.1021/la400971g.

[11] X. Zhang, C.L. Pint, M.H. Lee, B.E. Schubert, A. Jamshidi, K. Takei, H. Ko, A. Gillies, R. Bardhan, J. Urban, M. Wu, R. Fearing, A. Javey, Optically- and Thermally-Responsive Programmable Materials Based on Carbon Nanotube-Hydrogel Polymer Composites, Nano Lett. 11 (2011) 3239–3244. doi:10.1021/nl201503e.

[12] M. Dulle, S. Jaber, S. Rosenfeldt, A. Radulescu, S. Fo, P. Mulvaney, M. Karg, Plasmonic gold–poly(N-isopropylacrylamide) core–shell colloids with homogeneous density profiles: a small angle scattering study, Physical Chemistry Chemical Physics. 17 (2014) 1354–1367. doi:10.1039/C4CP04816D.

[13] T.A. Harroun, H. Fritzsche, M.J. Watson, K.G. Yager, O.M. Tanchak, C.J. Barrett, J. Katsaras, Variable temperature, relative humidity (0%–100%), and liquid neutron reflectometry sample cell suitable for polymeric and biomimetic materials, Review of Scientific Instruments. 76 (2005) 065101. doi:10.1063/1.1921550.

[14] X. Hu, Z. Tong, L.A. Lyon, Synthesis and Physicochemical Properties of Cationic Microgels Based on Poly(N-isopropylmethacrylamide), Colloid Polym Sci. 289 (2011)

333–339. doi:10.1007/s00396-010-2347-y.Synthesis.
[15] D. Suzuki, Y. Nagase, T. Kureha, T. Sato, Internal structures of thermosensitive hybrid microgels investigated by means of small-angle X□ray scattering, The Journal of Physical Chemistry. 118 (2014) 2194–2204. doi:10.1021/jp410983x.
[16] C. Wu, X. Wang, Globule-to-Coil Transition of a Single Homopolymer Chain in Solution, Physical Review Letters. 80 (1998) 4092–4094.
[17] S. Maccarrone, C. Scherzinger, O. Holderer, P. Lindner, M. Sharp, W. Richtering, D. Richter, Cononsolvency effects on the structure and dynamics of microgels, Macromolecules. 47 (2014) 5982–5988.
[18] R. Marcombe, S. Cai, W. Hong, X. Zhao, Z. Suo, A theory of constrained swelling of a pH-sensitive hydrogel, Soft Matt. 6 (2010) 784–793. doi:10.1039/b917211d.
[19] A. Suzuki, T. Tanaka, Phase transition in polymer gels indused by visible light, Nature. 346 (1990) 345–347.
[20] S. Ahn, R.M. Kasi, S. Kim, Y. Zhou, Stimuli-responsive polymer gels, Soft Matter. 4 (2008) 1151–1157. doi:10.1039/b714376a.
[21] W. Hong, X. Zhao, Z. Suo, Large deformation and electrochemistry of polyelectrolyte gels, Journal of the Mechanics and Physics of Solids. 58 (2010) 558–577. doi:10.1016/j.jmps.2010.01.005.
[22] M. Heskins, J.E. Guillet, Solution properties of poly(N-isopropylacrylamide), Journal of Macromolecular Science—Chemistry. A2(8) (1968) 1441–1455. doi:10.1080/10601326808051910.
[23] K. Kratz, T. Hellweg, W. Eimer, Structural changes in PNIPAM microgel particles as seen by SANS, DLS, and EM techniques, Polymer. 42 (2001) 6631–6639.
[24] M. Karg, S. Prévost, A. Brandt, D. Wallacher, R. v. Klitzing, T. Hellweg, Poly-NIPAM microgels with different cross-linker densities. Scaling behavior of the network fluctuations in thevicinity of the volume phase transition, Progress in Colloid and Polymer Science. 140 (2013) 63–76. doi:10.1007/978-3-319-01683-2.
[25] A. Burmistrova, R. v. Klitzing, Control of number density and swelling/shrinking behavior of P(NIPAM–AAc) particles at solid surfaces, Journal of Materials Chemistry. 20 (2010) 3502–3507. doi:10.1039/b923969c.
[26] M. Stieger, W. Richtering, J.S. Pedersen, P. Lindner, Small-angle neutron scattering study of structural changes in temperature sensitive microgel colloids, Journal of Chemical Physics. 120 (2004) 6197–6206. doi:10.1063/1.1665752.
[27] A.B. South, R.E. Whitmire, A.J. Garcıa, L.A. Lyon, Centrifugal Deposition of Microgels for the Rapid Assembly of Nonfouling Thin Films, ACS Appl. Mater. Interfaces. 1 (2009) 2747–2754. doi:10.1021/am9005435.
[28] A. Burmistrova, R. Steitz, R. v. Klitzing, Temperature Response of PNIPAM Derivatives at Planar Surfaces : Comparison between Polyelectrolyte Multilayers and Adsorbed Microgels, Minireviews. 11 (2010) 3571–3579. doi:10.1002/cphc.201000378.
[29] S. Schmidt, T. Hellweg, R. v. Klitzing, Packing Density Control in P(NIPAM-co-AAc) Microgel Monolayers: Effect of Surface Charge, pH, and Preparation Technique, Langmuir. 24 (2008) 12595–12602.
[30] S. Wellert, Y. Hertle, M. Richter, M. Medebach, D. Magerl, W. Wang, B. Demé, A. Radulescu, P. Müller-Buschbaum, T. Hellweg, R. v. Klitzing, Inner Structure of Adsorbed Ionic Microgel Particles, Langmuir. 30 (2014) 7168–7176.
[31] M.F. Schulte, A. Scotti, A.P.H. Gelissen, W. Richtering, A. Mourran, Probing the internal

heterogeneity of responsive microgels adsorbed to an interface by a sharp SFM tip – comparing core-shell and hollow microgels, Langmuir. 34 (2018) 4150–4158. doi:10.1021/acs.langmuir.7b03811.

[32] W. Su, K. Zhao, J. Wei, T. Ngai, Dielectric relaxations of poly(N-isopropylacrylamide) microgels near the volume phase transition temperature: impact of cross-linking density distribution on the volume phase transition, Soft Matter. 10 (2014) 8711–8723. doi:10.1039/C4SM01516A.

[33] A. Fernandez-Barbero, A. Fernandez-Nieves, I. Grillo, E. Lopez-Cabarcos, Structural modifications in the swelling of inhomogeneous microgels by light and neutron scattering, Physical Review E. 66 (2002) 051803. doi:10.1103/PhysRevE.66.051803.

[34] K. Kratz, T. Hellweg, W. Eimer, Influence of charge density on the swelling of colloidal poly (N -isopropylacrylamide-co-acrylic acid) microgels, Colloids and Surfaces A: Physicochemical and Engineering Aspects. 170 (2000) 137–149.

[35] T. Hellweg, C.D. Dewhurst, W. Eimer, K. Kratz, PNIPAM-co-polystyrene Core-Shell Microgels: Structure, Swelling Behavior, and Crystallization, Langmuir. 20 (2004) 4330–4335. doi:10.1021/la0354786.

[36] I. Berndt, W. Richtering, Doubly Temperature Sensitive Core-Shell Microgels, Macromolecules. 36 (2003) 8780–8785.

[37] R. Steitz, T. Gutberlet, T. Hauss, B. Klo, R. Krastev, S. Schemmel, A.C. Simonsen, G.H. Findenegg, Nanobubbles and Their Precursor Layer at the Interface of Water Against a Hydrophobic Substrate, Langmuir. 19 (2003) 2409–2418. doi:10.1021/la026731p.

[38] Heinz Maier-Leibnitz Zentrum, KWS-1 : Small-angle scattering diffractometer, Journal of Large-Scale Research Facilities. 1 (2015) 26–29.

[39] A. V. Feoktystov, H. Frielinghaus, Z. Di, S. Jaksch, H. Kleines, A. Ioffe, D. Richter, KWS-1 high-resolution small-angle neutron scattering instrument at JCNS : current state, Applied Crystallography. 48 (2015) 61–70. doi:10.1107/S1600576714025977.

[40] Heinz Maier-Leibnitz Zentrum, KWS-3 : Very small angle scattering diffractometer with focusing mirror, Journal of Large-Scale Research Facilities. 1 (2015) 8–10.

[41] G. Santoro, S. Yu, Grazing incidence small angle X-ray scattering as a tool for in-situ time-resolved studies, in: X-Ray Scattering, 2017: pp. 29–60.

[42] P. Müller-Buschbaum, Grazing incidence small-angle neutron scattering : challenges and possibilities, Polymer Journal. 45 (2013) 34–42. doi:10.1038/pj.2012.190.

[43] V. Lauter-Pasyuk, Neutron grazing incidence techniques for nano-science, Collection SFN. 7 (2007) s221–s240.

[44] P. Müller-Buschbaum, GISAXS and GISANS as metrology technique for understanding the 3D morphology of block copolymer thin films, European Polymer Journal. 81 (2016) 470–493. doi:10.1016/j.eurpolymj.2016.04.007.

[45] S. Nouhi, M.S. Hellsing, V. Kapaklis, A.R. Rennie, Grazing-incidence small-angle neutron scattering from structures below an interface, J. Appl. Cryst. 50 (2017) 1066–1074. doi:10.1107/S1600576717007518.

[46] M. Shibayama, Small-angle neutron scattering on polymer gels: phase behavior, inhomogeneities and deformation mechanisms, Polymer Journal. 43 (2010) 18–34. doi:10.1038/pj.2010.110.

[47] J. Bastide, L. Leibler, Large-scale heterogeneities in randomly cross-linked networks, Macromolecules. 21 (1988) 2647–2649. doi:10.1021/ma00186a058.

[48] S. Wellert, M. Richter, T. Hellweg, R. Von, R. Mikrogelpartikel, Responsive Microgels at

Surfaces and Interfaces, Z.Phys.Chem. (2014). doi:10.1515/zpch-2014-0568.

[49] T.A. Vilgis, J.F. Joanny, A. Johner, Polymer gels and brushes at surface, Macromol. Symp. 200 (2003) 67–80. doi:10.1002/masy.200351007.

[50] S. Matsui, Y. Nishizawa, T. Uchihashi, D. Suzuki, Monitoring thermoresponsive morphological changes in individual hydrogel microspheres, ACS Omega. 3 (2018) 10836–10842. doi:10.1021/acsomega.8b01770.

[51] T. Kyrey, M. Ganeva, K. Gawlitza, J. Witte, R. Von Klitzing, O. Soltwedel, Z. Di, S. Wellert, O. Holderer, Grazing incidence SANS and reflectometry combined with simulation of adsorbed microgel particles, Physica B: Physics of Condensed Matter. 551 (2018) 172–178. doi:10.1016/j.physb.2018.03.049.

Highlights:

- Characterization of different length scale internal inhomogeneities with GISANS
- Influence of the cross-link concentration on layer formation at solid substrate
- Microgel inner structure below and above VPTT in adsorbed state
- Combination of methods for microgel structure investigation at solid-liquid interface.